Locational activated PRP via injectable double-network hydrogel for endometrial regeneration

Jia Qi[1,2,10], Xiaoxiao Li[3,4,5,6,10], Yumeng Cao[1,2,10], Yijing Long[1,2], Junliang Lai[1,2], Yejie Yao[1,2], Yiwen Meng[1,2], Yuan Wang[1,2], Xiao-Dong Chen[7,8], Hugo Vankelecom[9], Xuejiao Bian[9], Wenguo Cui[3,4,5,*], Yun Sun[1,2,11,*]

[1]Center for Reproductive Medicine, Ren Ji Hospital, Shanghai Jiao Tong University School of Medicine, Shanghai, China

[2]Shanghai Key Laboratory for Assisted Reproduction and Reproductive Genetics, Shanghai, China

[3]Department of Orthopaedics, Ruijin Hospital, Shanghai Jiao Tong University School of Medicine, Shanghai, China

[4]Shanghai Key Laboratory for Prevention and Treatment of Bone and Joint Diseases, Ruijin Hospital, Shanghai Jiao Tong University School of Medicine, Shanghai, China

[5]Shanghai Institute of Traumatology and Orthopaedics, Ruijin Hospital, Shanghai Jiao Tong University School of Medicine, Shanghai, China

[6]Laboratory of Key Technology and Materials in Minimally Invasive Spine Surgery, Tongren Hospital, Shanghai Jiao Tong University School of Medicine, Shanghai, China

[7]Department of Comprehensive Dentistry, University of Texas Health Science Center at San Antonio, San Antonio, TX 78229, U.S.A

[8]Research Service, South Texas Veterans Health Care System, Audie Murphy VA Medical Center, San Antonio, TX, 78229, U.S.A

[9]Department of Development and Regeneration, Cluster Stem Cell Biology and Embryology, Research Unit of Stem Cell Research, University of Leuven (KU Leuven), B-3000 Leuven, Belgium

[10]These authors contributed equally.

[11]Lead contact

*Correspondence: syun163@163.com (Y.S.), wgcui80@hotmail.com (W.C.)

SUMMARY

Background: Enhancing the therapeutic effectiveness of platelet-rich plasma (PRP) for endometrial regeneration presents a challenge, due to the need for precise locational activation of PRP. Here, an injectable interpenetrating double-network hydrogel, characterized by intrauterine locational activation of PRP, is developed by dynamic borate bonds and photo-crosslinking. This PRP-hydrogel prevents endometrial fibrosis and promotes angiogenesis, thereby facilitating endometrial regeneration.

Methods: The dynamic borate bonds formed instantaneously between methacrylated hyaluronic acid -phenylboronic acid (HAMA-PBA) chelating Ca^{2+} with carboxyl and polyphenol groups, and poly(vinyl alcohol) (PVA) loaded with PRP. This, combined with photo-crosslinking, facilitated the intrauterine locational activation of PRP, the sustained release of growth factors, and an

increase in the uterine retention rate of PRP.

Findings: *In vitro* experiments demonstrated that PRP-hydrogel considerably encouraged the proliferation of endometrial cells and manifested robust proangiogenic properties, resulting in comprehensive reparation of the endometrial microenvironment. The PRP-hydrogel regulated the expression of collagen deposition genes by inhibiting the TGFβ1-SMAD2/3 pathway, thereby suppressing endometrial fibrosis. Furthermore, *in vivo* experiments using intrauterine adhesion (IUA) model rats treated with PRP-hydrogel demonstrated significant promotion of endometrial regeneration and functional remodeling. The IUA model rats almost completely recovered under PRP-hydrogel treatment, with a substantial increase in embryo implantation numbers, litter size, and live birth rate, similar to normal rats.

Conclusion: Overall, this injectable double-network hydrogel, capable of locational activation of PRP, offers a promising new therapeutic strategy for endometrial repair in IUA patients.

Funding: This work was supported by the National Key R & D Program of China (2023YFC2705500).

Keywords: Locational activation; Platelet-rich plasma; Injectable hydrogel; Phenylborate ester reaction; Endometrial regeneration; Intrauterine adhesion

INTRODUCTION

Intrauterine adhesion (IUA), a gynecological disorder, is typified by varying degrees of adhesion or obstruction in the uterine cavity post-endometrial injury[1,2]. IUA is a leading cause of uterine infertility, profoundly affecting the endometrial receptivity to embryos. The incidence of IUA reaches 19% after miscarriage surgery, and the incidence of IUA following hysteroscopic electrosurgery is even higher, ranging from 20% to 62.5%[3,4]. The current standard treatment for IUA is transcervical resection of adhesion (TCRA), supplemented with various adjunctive therapies such as physical barriers (contraceptive devices, intrauterine balloon devices, etc.) to prevent postoperative adhesion, and estrogen therapy to stimulate endometrial regeneration[5-7]. Nevertheless, evidence suggests that physical barriers alone are insufficient to prevent IUA recurrence[8]. Systemic estrogen application may elevate the risk of thrombosis and breast cancer[9,10], and its limited half-life results in a low effective concentration in the damaged endometrium. As a result, the recurrence incidence of post-surgery adhesion in IUA patients is significant due to a lack of efficient treatment. Endometrial growth in IUA patients is slow and asynchronous with embryonic development, making treatment far from satisfactory. Thus, the prevention and treatment of IUA have become a bottleneck issue in reproductive medicine.

Under physiological circumstances, the endometrium undergoes proliferation and shedding synchronously with the menstrual cycle, culminating in a scarless repair[11]. The pathological development of IUA involves a vicious cycle that influences endometrial cell proliferation, endometrial angiogenesis, and subsequently endometrial fibrosis, thereby increasing the severity of adhesion[12]. IUA is not a disease triggered by a single factor, but a complex endometrial disorder

induced by widespread alterations in the microenvironment[13]. Since systemic medications have undesirable side effects, emphasizing enhancing the endometrial local microenvironment and achieving locational endometrial treatment is pivotal to IUA therapy[14]. Locational endometrial treatment not only avoids potential side effects caused by systemic medication but also enhances the concentration of effective medicine, thus promoting the healing of endometrium[15]. However, it is difficult to obtain satisfactory therapeutic results with intrauterine drug perfusion alone. Since the uterus, as a hollow organ with an opening to the vagina via the cervical canal, permits the fluid drug to easily flow out of the uterine cavity when the body position shifts to an upright position, making it challenging for drug retention[16]. Moreover, the uterine cavity, with a capacity of merely 5ml, limits the amount of locally infused drugs. An excessively high local drug concentration may induce uneven overgrowth of the local endometrium. Therefore, it is crucial to attain precise locational endometrial therapy with medications in a manageable concentration to treat IUA effectively.

Owing to its exceptional tissue regeneration capabilities, platelet-rich plasma (PRP) is progressively attracting the interest of clinicians for its potential to augment endometrial function. However, previous clinical studies examining the application of PRP in the endometrium have yielded inconsistent results[17-19]. This divergence may be attributed to certain limitations of PRP's efficacy within the uterine cavity[20]: 1) PRP itself has very limited mechanical properties, which is easily metabolized and collapsed; 2) PRP needs extra activation using thrombin and calcium chloride. Upon activation, PRP instigates a cascade release of growth factors (GFs), which is transient and inadequate for endometrial regeneration. 3) Once activated, PRP will form a gel-like state, which cannot be injected, resulting in incomplete filling of irregular damage and posing usage difficulties. Therefore, enhancing the stability and injectability of PRP, ensuring the sustained release of growth factors, and augmenting its retention rate in the uterus is crucial for optimizing the effectiveness of PRP. Recent advancements in tissue engineering and regenerative medicine have facilitated the extensive use of treatments that combine biomaterials and PRP, including orthopedic regenerative therapy, skin wound repair, and hair regeneration. Zhou et al. utilized hyaluronic acid and ε-polylysine to load activated PRP, leveraging the lyophilized hydrogel scaffold's macropore barrier[21]. Cai et al. constructed a composite adhesive hydrogel by incorporating bacterial cellulose and activated PRP into a poly-N-(tris[hydroxymethyl]methyl)acrylamide (THMA)/N-acryloyl aspartic acid (AASP) hybrid gel network [22]. Jiang et al. created a gelatin methacryloyl (GelMA) hydrogel scaffold with varying PRP concentrations, employing the digital micro-mirror device technique for osteochondral repair[23]. Currently, PRP-relevant hydrogels are seldomly designed for hollow organs with an opening, lacking sufficient self-repair capacities and in situ locational activation, usually grapple with the challenge of sudden cytokine release from PRP. Hence, it is of great significance to develop a multifunctional PRP-loaded hydrogel with injectability, self-healing, intrauterine locational activation and sustained GFs' release, which are desirable for extensive application in the management of IUA.

Based on the characteristics of IUA and PRP, we created and developed locational activated PRP via injectable, porous-like, degradable dual-network hydrogels with multiple advantages, including rapid gelation, self-healing, pro-proliferation, pro-angiogenesis and anti-fibrosis. As illustrated in Figure 1, a methacrylated hyaluronic acid (HAMA)-phenylboronic acid (PBA) monomer was first synthesized by copolymerization of HAMA and PBA complex. The carboxy groups and polyphenol groups provided by PBA were used to chelate Ca^{2+}, for locational PRP activation. Meanwhile, PRP was loaded in poly(vinyl alcohol) (PVA) by physical combination mode. Subsequently, a 3D gel network was created by mixing HAMA-PBA and PVA together, utilizing the dynamic boronic ester link between boronic acid and 1,3-diol groups. Thereafter, UV light could initiate the photo-crosslinking of HAMA polymer, forming a secondary network, thus establishing the locational activated PRP@HAMA-PBA-PVA hydrogel system (noted as PRP@GEL). This system employs the primary network, built via dynamic borate bonds, to foster the interaction between Ca^{2+} and PRP within the gel network. This interaction facilitates the continuous locational activation of PRP and the subsequent sustained release of growth factors, while also improving self-healing capabilities. The secondary network, established through photo-crosslinking, augments both the adhesion and mechanical attributes of the composite material *in vivo*. Ultimately, this system enables the locational activation of PRP in the impaired endometrium of IUA, thereby fully utilizing the advantages of PRP and delivering sustained therapeutic factors in endometrial regeneration. It harmonized the endometrial microenvironment by sustained release of growth factors from PRP, contributing to endometrial regeneration and fertility restoration. *In vitro* studies have revealed that PRP@GEL significantly enhances endometrial cell proliferation and exhibits notable pro-angiogenic effects, thereby inducing comprehensive repair of the endometrial microenvironment. PRP@GEL modulates the expression of collagen deposition genes by inhibiting the TGFβ1-SMAD2/3 pathway, consequently suppressing endometrial fibrosis. Furthermore, *in vivo* experiments conducted on IUA model rats treated with PRP@GEL have significantly promoted endometrial regeneration and functional remodeling. IUA model rats demonstrated nearly complete recovery following PRP@GEL treatment. This was evidenced by a significant increase in the number of embryo implantations, litter size, and live birth rate, which were comparable to those of normal rats. This injectable dual-network hydrogel, capable of localized activation of PRP, offers a promising new therapeutic strategy for endometrial repair in uterine cavity adhesions.

RESULTS AND DISCUSSION

Design and synthesis of the HAMA-PBA conjugate

A two-step process was used to synthesize HAMA-PBA. First, HAMA was obtained by grafting methacrylic to hyaluronic acid via an esterification reaction. Second, HAMA-PBA was synthesized by grafting 3-aminophenylboronic acid to hyaluronic acid via an amidation reaction (Figure 2A). In Figure 2B, the ^{1}H NMR spectrum demonstrated that HA has successfully been dual-modified. Proton signals at 5.71 and 6.09 ppm correspond to vinyl characteristics of

methacrylic acid, whereas those at 7.45, 7.49, 7.64 and 7.86 ppm correspond to benzene rings characteristic of phenylboronic acid.

Characterization of the dual crosslinked, injectable, porous, and self-healing hydrogel

Given the fluidity of PRP, its low retention rate, and the subsequent rapid release of GFs following intrauterine perfusion, the therapeutic effect of PRP may not be sustained for an extended period within the uterine cavity[24]. Here, a PRP-loaded dual crosslinked hydrogel was designed. Firstly, the HAMA-PBA monomer is prepared through the amide reaction. The carboxy and polyphenol groups provided by HAMA-PBA are used to load Ca^{2+} through chelation. The PRP was loaded in PVA via physical combination. Then, a 3D gel network in situ was formed by mixing the HAMA-PBA solution and PVA-PRP mixture solution together at PH 8.5. As a result of the dynamic boronic ester bond, rapid gelation occurred within 20 seconds at room temperature. Subsequently, the photo-crosslinking of the HAMA polymer chains is initiated by UV light, forming a secondary network to enhance the cross-linking degree and stability of the hydrogel, and finally obtained PRP@HAMA-PBA-PVA hydrogel (noted as PRP@GEL) (Figure 2C). While without PRP loading, the HAMA-PBA-PVA hydrogel was fabricated (noted as GEL). The hydrogel developed in the present study, PRP@GEL, has enhanced mechanical strength and quick self-healing ability, which enables the maintenance of structural integrity during the intrauterine endometrial regeneration process. As a result, it creates a pristine and moist environment that hastens the process of endometrial regeneration. Meanwhile, the self-repair abilities of the hydrogels may lead to a quick reinstatement of the hydrogel infrastructure following rupture and guarding the bioactivity of the vulnerable PRP [25], that has been loaded. This is advantageous for the regeneration of the endometrium.

Injectability is crucial for treating IUA. As demonstrated in Figure 2D, PRP@GEL can be effortlessly injected using a 21G needle with no blockages and promotes rapid healing. It is versatile and can adapt to irregular tissue defects. Furthermore, PRP@GEL could self-degrade in 14 days (Figure 2D).

Figure 2E showed the rheological characterization and the self-repairable properties of the hydrogel and the difference between single-network hydrogel and double-network hydrogel. Firstly, when oscillatory strain sweep was conducted on the single-network hydrogel without UV light crosslinking, the storage modulus of the single-network hydrogel was 120Pa (Figure 2E-i). After subjecting the single-network hydrogel to UV light irradiation in a time gradient manner, we found that the modulus of the hydrogel could be significantly increased with the extension of UV light exposure time (Figure 2E-ii). Subsequently, when oscillatory strain sweep was conducted on the double-network hydrogel that had been crosslinked with UV light for 20s, the storage modulus of the double-network hydrogel increased to 300Pa (Figure 2E-iii). The cyclic experiments of shear strain moving between 1% and 1000% showed that the self-healing performance has

excellent repeatability (Figure 2E-iv).

SEM revealed that the single-network hydrogel before UV irradiation displayed a uniform honeycomb-like porous structure. After photo-crosslinking, the double-network hydrogel demonstrated that the crosslinking density increased, the pore size decreased, and the porous structure became more compact (Figure 2F).

PRP@GEL is capable of sustained release of growth factor *in vitro*

PRP contains various GFs, including platelet-derived growth factor (PDGF), vascular endothelial growth factor (VEGF) and epidermal growth factor (EGF). These GFs have the potential to positively impact the endometrial regeneration process.[26,27]. However, the sudden release of these GFs after PRP activation restricts its application. Locational PRP activation and incorporation of GFs into hydrogels is seen as a promising approach for exhibiting a prolonged GFs' release to enhance the effectiveness of endometrial regeneration [28,29]. Herein, PRP was loaded into the HAMA-PBA-PVA hydrogel via dynamic borate bonds and photo-crosslinking. The Ca^{2+} chelated by carboxy and polyphenol groups provided by HAMA-PBA was used for locational PRP activation and the growth factors released from PRP activation could be encapsulated into 3D hydrogels to further guarantee the sustained release of GFs.

The detection of GFs, including PDGF, VEGF, and EGF, was conducted in order to comprehend the impact of the hydrogel on GFs' release. The GFs were detected using Enzyme-linked immune sorbent assay (ELISA) method, after hydrogels were immersed in PBS for different time. As shown in Figure 3A, B and C, explosive release of GFs occurs from PRP within the initial 24 hours, while the equilibrium release is detected after 72 hours. In contrast, sustained release behaviors of GFs are observed from the PRP@GEL, this can be due to the locational activation and encapsulation of PRP via double-network hydrogel.

Biocompatibility and proliferative function of PRP@GEL

To better promote the clinical application of hydrogels, biocompatibility is crucial [30]. Since the mechanisms of IUA consist of insufficient cell proliferation, decreased angiogenesis, and aberrant fibrosis[31], we used primary human endometrial stromal cells (HESCs) and human umbilical vein endothelial cells (HUVECs) for further biocompatibility experiments.

To assess the cytotoxicity of GEL and PRP@GEL hydrogels, the CCK-8 assay and EdU staining were used to analyze cell survival following coculturing hydrogels with cells. As shown in Figure 3D and E, all groups exhibited no inhibition of cell proliferation both in HESCs and HUVECs. Notably, in HESCs the absorbance of the PRP@GEL group was significantly higher than that of the PRP, GEL and CTRL group at day3 ($p < 0.05$). In HUVECs, the absorbance of the PRP@GEL group and PRP group were both higher than that of CTRL group at day3 ($p < 0.05$). Additionally, the EdU staining of HESCs and HUVECs also showed the same pattern, where more proliferative cells (red) were observed in the PRP@GEL group compared to CTRL group (Figure 3F-I). These

results indicated that PRP-containing hydrogels did not exhibit cytotoxicity towards HESCs and HUVECs but promote cell proliferation.

Regulation of fibrosis signaling by PRP@GEL

Endometrial fibrosis is one of the main pathological features of IUA[32]. Therefore, anti-fibrosis is important for both treating and preventing IUA[33]. To investigate the *in vitro* effects of PRP@GEL in endometrial fibrosis, HESCs were isolated in accordance with our earlier research [34,35]. Previous researches have demonstrated a significant increase in TGF-β1 within the endometria of IUA patients [36,37]. It has been postulated that the increased expression of TGF-β1 contributes to the development and progression of fibrosis in IUA. The degree of endometrial fibrosis has been shown to align with the expression level of TGF-β1 during IUA formation.

Here, we simulated the potential microenvironmental challenge that HESCs could encounter within the endometrium through treatment with TGF-β1. Conditioned medium immersed with GEL, PRP, and PRP@GEL hydrogels were used to treat TGF-β1 induced *in vitro* fibrosis model (Figure 4A). The *in vitro* anti-fibrosis effects were examined through the detection of expression levels in corresponding genes. The possible signaling pathway underline the fibrosis prevention was further explored. When stimulating HESCs with TGF-β1, the mRNA expression of fibrosis markers including COL1A1, α-SMA and CTGF were upregulated significantly (Figure 4B-D), indicating successfully induced *in vitro* fibrosis model. The treatment of GEL alone did not affect the expression upregulation of TGF-β1 induced COL1A1, α-SMA and CTGF. The treatment of PRP alone could partially decrease the expression of COL1A1 without significant effect but do not change the expression of α-SMA and CTGF. When treated with PRP@GEL, the expression of COL1A1, α-SMA and CTGF were significantly downregulated (Figure 4B-D). The result of western blot (WB) revealed the consistent results. TGF-β1 stimulated the protein expression of COL1A1, α-SMA and CTGF while PRP@GEL could effectively downregulate the TGF-β1 induced COL1A1, α-SMA and CTGF (Figure 4E-H). Phosphorylation of SMAD2/3 is one of the essential signaling pathway in fibrosis formation. In the TGF-β1 group, the expression of p-SMAD2/3 and phosphorylation of SMAD2/3 were upregulated. After treated with PRP@GEL, the expression of p-SMAD2/3 and phosphorylation of SMAD2/3 were significantly decreased (Figure 4I-L), indicating PRP@GEL could deactivate TGF-β1-SMAD2/3 pathway in *in vitro* fibrosis model. To summarize, PRP@GEL could downregulate the expression of fibrosis genes via deactivating TGF-β1-SMAD2/3 signaling pathway, thus regulating the fibrosis of HESCs.

Regulation of angiogenesis by PRP@GEL

Angiogenesis plays a vital role in IUA recovery, and the treatments targeted angiogenesis were proved to be efficacious for IUA[38]. Angiogenesis is a multifaceted process comprising multiple steps. Endothelial cells undergo activation when exposed to angiogenic stimuli, leading to degradation of the basement membrane and subsequent sprouting, migration, and proliferation to create capillary tube branches that eventually join with adjacent vessels [39]. Herein, the regulation

of angiogenesis was assessed in HUVEC cells. The proliferative effect of PRP@GEL on HUVECs has already been proved in previous part. Wound healing experiments showed that the PRP@GEL group healed 86.65 ± 2.90% at 12h compared to 54.69 ± 5.00% in the CTRL group ($p < 0.001$), indicating better cell migration in the PRP@GEL-treated group (Fig. 5A and 5B). Transwell invasion assays revealed that PRP treatment significantly enhanced HUVECs invasion, and this effect was further enhanced for PRP@GEL treatment (Figure 5C and 5D). Endothelial cell tube formation assay revealed the angiogenic effect of PRP@GEL treatment. The number of junction, number of master junction, number of master segments, number of segments, and segments lengths were all enhanced in PRP@GEL group compared with CTRL group (Figure 5E-J). Meanwhile, the generally acknowledged angiogenic genes including VEGFA and PDFGA were increased in PRP@GEL group, while FSTL1 and ANGPT2 showed increasing trend without significance in PRP@GEL group (Figure 5K-N). In summary, PRP@GEL could promote angiogenesis thereby enhancing endometrial regeneration and IUA recovery.

***In vivo* endometrial regeneration effects by PRP@GEL in IUA rats**

An animal model of IUA was constructed via injecting 95% ethanol into the uterine horn in SD-rats to evaluate the *in vivo* effects of PRP@GEL[40]. The female rats were randomly divided into five groups as the details mentioned in STAR methods.

Briefly, the CTRL group was created by injecting PBS to simulate the surgical procedure (sham-operation). The IUA models were therapied with PBS (ETOH group), GEL (GEL group), PRP (PRP group), and PRP@GEL (PRP@GEL group), respectively for 2 weeks (Figure 6A). On postoperative 14th day, fourteen rats per group were sacrificed, and the gross images and tissue section staining of the uterus were captured and analyzed. Compared with the CTRL group, the damaged uterine tissue in the ETOH group showed a significant thinning of the endometrium with scarce glands. In the PRP@GEL group, the stroma and epithelium were well distributed, and the endometrial thickness and gland number increased (Figure 6B-G). Specifically, in the CTRL group, the average endometrium thickness was 440.9 μm with 17.25 glands. However, in the ETOH group, the endometrium thickness was only 329.0 μm with only 2.69 glands. In contrast, the average endometrial thickness in PRP@GEL group was 449.3 μm with an average of 16.38 glands, which showed the remarkable tissue regeneration capability of the PRP@GEL (Figure 6F and 6G). Meanwhile, the average thickness of uterus and number of glands in PRP@GEL group were higher than that in the PRP group as well (Figure 6F and 6G) which indicated that PRP@GEL had a better effect of promoting endometrial repair.

Through *in vitro* cell experiments, we observed the protective effect of PRP@GEL in *in vitro* fibrosis model. To further evaluate *in vivo* anti-fibrosis in rat, we conducted Masson's trichrome staining in five groups to examine endometrial collagen deposition. A significant increase in endometrial collagen deposition was seen in the ETOH group (average collagen staining 28.88%), which was significantly higher than that in the CTRL group (average collagen staining 7.88%). In contrast, PRP@GEL group (average collagen staining 8.04%) exhibited a 20.84% reduction in

collagen deposition compared with the ETOH group and 12.25% reduction compared with the PRP group (Fig. 6D and 6H). The protein expression of fibrosis maker (α-SMA and COL1A1) in endometrial areas revealed consistent results. The α-SMA positive area was increased in the ETOH group but decreased in the GEL, PRP and PRP@GEL group (Figure 7A and 7B). The COL1A1 positive area was increased in the ETOH group while it was reduced in the PRP@GEL group only (Figure 7C and 7D). These findings collectively demonstrate the effectiveness of PRP@GEL in alleviating endometrial fibrosis and reducing collagen deposition.

As endometrial regeneration relies on angiogenesis to regenerate tissue[41], we aimed to investigate if there was a correlation between the PRP@GEL-induced neovascularization observed *in vitro* (Figure 5) and endometrial angiogenesis *in vivo*. Immunohistochemistry staining of the rat uterus showed higher expression of CD31 and vWF in the PRP@GEL group compared to the ETOH group (Figure 7E-H). The above results indicated that PRP@GEL increased angiogenesis.

Above all, PRP@GEL could effectively increase endometrial thickness, relieve endometrial fibrosis, and increase angiogenesis.

PRP@GEL increased the implantation rates and live birth rates in IUA rats

Fertility restoration is considered as the ultimate purpose in endometrial function regeneration[42]. Above results have proved the effective ability of PRP@GEL in endometrial regeneration of IUA rats, whether PRP@GEL could restore the fertility of rats with IUA is necessary to explore. Here, a comprehensive fertility experiments involving embryo implantation, embryonic development, and live births were carried out. On the 14th day after the operation, the female SD rats were paired 1:1 with SD male mice, and the mating success was determined by morning vaginal smear. Eight rats per group were euthanized on the 14 days post-coitum (dpc), and the uterus were collected to analyze the number of implanted embryos and implantation rate. The number of implantation sites in the ETOH group (1.38 ± 0.89) was significantly lower than the CTRL group (12.50 ± 1.12), while the number of implantation sites in PRP@GEL (8.38 ± 1.67) was significantly higher than that in ETOH group and was comparable with that in the CTRL group (Figure 8A and 8C). Eight female rats per group were continued feeding and the number of fetuses revealed consistent results. The number of fetuses reduced significantly in the ETOH group (1.13 ± 0.79) while PRP@GEL could restore the damaged endometrial function and the number of fetuses in the PRP@GEL group (6.88 ± 1.54) was significantly increased than that in the ETOH group and comparable with that in the CTRL group (10.63 ± 1.09) (Figure 8B and 8D). When compared with the CTRL group, the live birth rate in the ETOH group (25%) showed a sharp decrease and the live birth rate in the PRP@GEL group reached 87.5% (Figure 8E). There was no difference in the average weight of fetuses among different groups (Figure 8F). In addition, we monitored the development of offspring in the PRP@GEL group and found normal neonatal growth over a 14-day period (Figure 8G).

These findings indicated that intrauterine administration of PRP@GEL substantially increased the number of live births in rats with uterine damage without no adverse effect on the growth and

development of the offspring.

In summary, we developed and produced locational-activated PRP via injectable double-network hydrogels (PRP@GEL) through a conjugation reaction of HAMA-PBA and PVA utilizing the dynamic boronic ester bond and photo-crosslinking. The specific fabrication and structure enabled the intrauterine locational activation of PRP and sustained release of growth factors, while preventing the cascade release and rapid clearance of active growth factors. The PRP@GEL hydrogels were proven to possess the properties of pro-proliferation, pro-angiogenesis, anti-fibrosis and comprehensive repair of the endometrial microenvironment. Cellular experiments revealed that PRP@GEL hydrogels could promote endometrial cell proliferation, facilitate angiogenesis and inhibit the TGFβ1-SMAD2/3 pathway in HESCs to regulate the expression of collagen deposition genes, thereby suppressing endometrial fibrosis. The *in vivo* experiments confirmed that PRP@GEL hydrogels could enhance endometrial regeneration and improve live birth rates. Thus, the creation of locational-activated PRP via injectable double-network hydrogels offers a new and promising approach to IUA therapy and displays potential for tissue regeneration in a variety of applications.

Limitations of study

The endometrium plays a crucial role in facilitating embryo implantation. In order to adhere to ethical guidelines pertaining to the safety of both mothers and infants, this study exclusively conducted in vivo endometrial repair experiments utilizing PRP@GEL on rat models rather than on patients with intrauterine adhesions (IUA). The findings obtained from these experiments on IUA rats may offer valuable insights into the potential efficacy of PRP@GEL for future in vivo human endometrial repair. In order to investigate the role of PRP@GEL in the repair of human endometrial injury, it is imperative to conduct a more thorough evaluation of the biocompatibility of PRP@GEL. This will facilitate a deeper exploration into the possibility of achieving similar outcomes in patients with intrauterine adhesions (IUA). Additionally, it is essential to undertake more rigorous clinical randomized controlled trials to gather conclusive evidence in this regard.

Acknowledgements

This study was supported by the National Key R＆D Program of China (2023YFC2705500, 2023YFC2705505, 2019YFA0802604), National Natural Science Foundation of China (82130046, 82320108009, 81901550, 52103174, 82101747) , Shanghai leading talent program, Innovative research team of high-level local universities in Shanghai (SHSMU-ZLCX20210201, SSMU-ZLCX20180401), Shanghai "Rising Stars of Medical Talents" Youth Development Program Youth Medical Talents (SHWSRS(2023)_062), Shanghai Jiao Tong University School of Medicine Affiliated Renji Hospital Clinical Research Innovation Cultivation Fund Program (RJPY-DZX-003) and Shanghai Pujiang Program (2021PJD044).

Author contributions

Conceptualization, J.Q., X.L., Y.S. and W.C.; Methodology, J.Q., Y.C. and X.L.; Analysis, J.Q.; Investigation, J.Q., Y.C., X.L., Y.L., J.L., Y.Y., X.B. and Y.M.; Resources, J.Q., Y.C. and X.L.; Writing-Original Draft, J.Q., Y.C., and X.L; Writing-Review & Editing, W.C., Y.S., X.C and H.V.; Visualization, J.Q., Y.C. and X.L.; Supervision, Y.S. and W.C.; Funding Acquisition, Y.S., J.Q., X.L. and Y.W..

Declaration of interests

The authors declare no competing interests.

Figure legends

Figure 1. The schematical illustration of locational activated PRP via injectable double-network hydrogel (PRP@HAMA-PBA-PVA). (A) Fabrication of HAMA-PBA and PRP@HAMA-PBA-PVA. (B) The rapid gelation of double network hydrogels, in situ positioning activation of PRP and sustainable release of growth factors. (C) When perfused intrauterine, PRP@HAMA-PBA-PVA could promote endometrial cell proliferation and angiogenesis, alleviate fibrosis, and therefore restore endometrial function and facilitate embryo implantation.

Figure 2. Characterization of the hydrogels. (A) The synthesis and scheme of HAMA-PBA. **(B)** The ^{1}H NMR spectra of HAMA-PBA. **(C)** schematic illustration of in situ activated PRP loaded HAMA-PBA-PVA. **(D)** The photographs demonstrated the injectable and degradable ability of PRP@HAMA-PBA-PVA. **(E)** Characterization of the rheological properties of PRP@HAMA-PBA-PVA. i) strain sweep measurements of G' (storage modulus) and G'' (loss modulus) of hydrogels before UV irradiation single network PRP@HAMA-PBA-PVA. ii) the time-dependant changes of G' and G'' under UV irradiation. Iii) strain sweep measurements of G' and G'' of hydrogels after UV irradiation double network PRP@HAMA-PBA-PVA. **(F)** SEM images of hydrogels before photo-crosslinking and after photo-crosslinking. SEM images of i) before UV irradiated single network PRP@HAMA-PBA-PVA and ii) after UV irradiated double network PRP@HAMA-PBA-PVA. Bar= 100 μm, 50 μm, 20 μm and 5μm.

Figure 3. The cumulative release curves of growth factors and *in vitro* cytocompatibility of the hydrogels. (A-C) Release kinetic curves of PDGF **(A)**, EGF **(B)** and VEGF**(C)** in PRP and double network PRP@HAMA-PBA-PVA hydrogels (notes as PRP@GEL). **(D and E)** The proliferation of **(D)** HESCs and **(E)** HUVECs were measured by CCK-8 assay from day 0 to day 3 when cocultured with medium only (CTRL), double network HAMA-PBA-PVA (GEL), PRP and PRP@GEL. n=4. **(F-I)** Immunofluorescent staining of EdU (red) of HESCs (F) and HUVECs (H), and the statistical EdU positive rate among CTRL, GEL, PRP and PRP@GEL. n=6. Data are means ± SEM, *P < 0.05, **P < 0.01, ***P < 0.001.

Figure 4. Effects of PRP@GEL on *in vitro* fibrosis of HESCs. (A) The schematic illustration of in vitro HESCs fibrosis model construction and the rescue treatment. **(B-D)** The qRT-PCR approach was used to assess the mRNA expression of COL1A1, α-SMA and CTGF, with GAPDH serving as a normalization control. n=4. **(E-H)** Western blotting was used to assess the protein expression of COL1A1, α-SMA and CTGF. The representative western blotting images and

statistical results are showed. n=4. **(I-L)** Western blotting was used to assess the activation of phosphorylated SMAD2/3. The representative western blotting images and statistical results are showed. n=4. Data are means ± SEM, *P < 0.05, **P < 0.01, ***P < 0.001.

Figure 5. Effects of PRP@GEL on the migration, invasion and angiogenesis of HUVECs. (A-B) Representative bright-field images and quantitative analysis of HUVECs after treated with GEL, PRP and PRP@GEL. n=4. **(C-D)** The microscopic images and quantitative analysis of invaded HUVECs. n=4. **(E)** Representative images of *in vitro* formed tubes in HUVECs under treatment of GEL, PRP and PRP@GEL. **(F-J)** Quantitative analysis of tube intensity in different evaluation indexes. n=6. (K-N) The qRT-PCR approach was used to assess the mRNA expression of VEGFA, PDGFA, FSTL1 and ANGPT2, with GAPDH serving as a normalization control. n=4. Data are means ± SEM, *P < 0.05, **P < 0.01, ***P < 0.001.

Figure 6. *In vivo* effects of PRP@GEL in restoration of endometrial thickness and fibrosis. (A) The schematic illustration of *in vivo* IUA model construction and rescue treatment after endometrial damage. **(B)** Representative mages of the isolated uterus of rats on the 14th day after surgery with different rescue treatment. CTRL: without endometrial damage. ETOH: with ETOH endometrial damage but without rescue treatment. GEL: rescue with GEL only after endometrial damage. PRP: rescue with PRP only after endometrial damage. PRP@GEL: rescue with PRP@GEL after endometrial damage. **(C)** Histological structures of uterine endometrial with HE straining. **(D)** Masson's trichrome staining was used to evaluate endometrial fibrosis (blue, consistent with scar formation). **(E)** Quantitative analysis of endometrial thickness in each group. n=14. **(F)** Quantitative analysis of number of glands in each group. n=14. **(G)** Quantitative analysis of fibrosis area ration. n=14. Data are means ± SEM, *P < 0.05, **P < 0.01, ***P < 0.001.

Figure 7. *In vivo* effects of PRP@GEL in endometrial collagen deposition. (A-B) Representative immunohistochemical staining images and quantification of α-SMA as a fibrosis marker. n=14. **(C-D)** Representative immunohistochemical staining images and quantification of COL1A1 as a fibrosis marker. n=14. **(E-F)** Representative immunohistochemical staining images and quantification of CD31 as an angiogenesis marker. n=14. **(G-H)** Representative immunohistochemical staining image and quantification of vWF as an angiogenesis marker. n=14. Data are means ± SEM, *P < 0.05, **P < 0.01, ***P < 0.001.

Figure 8. Pregnancy outcomes of different inventions. (A) Representative images of embryo implantation sites in the different groups. (B) Representative images of live births of pregnant mice in different groups. (C) Quantification of number of embryo implantation sites of different groups. n=8. (D) Quantification of number of fetuses of different groups. n=8. (E) Live birth rate of different groups. n=8. (F) Quantification of average weight of fetuses. n=8. (G) Images of newborn rats in PRP@GEL group after feeding 14 days. Data are means ± SEM, *P < 0.05, **P < 0.01, ***P < 0.001.

STAR Methods

- KEY RESOURCES TABLE
- RESOURCE AVAILABILITY
  - Lead contact
  - Materials availability
  - Data and code availability
- EXPERIMENTAL MODEL AND SUBJECT DETAILS
  - Endometrial tissue acquisition, cell isolation and cell culture
  - *In Vivo* IUA Model Construction and Treatment
- METHOD DETAILS
  - Materials and synthesis
  - Characteristics of the hydrogels
  - Preparation of PRP
  - *In Vitro* Growth Factor Release Kinetics
  - *In Vitro* Cell Proliferation Experiments
  - *In Vitro* Fibrosis and Anti-fibrosis Experiments
  - *In Vitro* Angiogenesis Experiments
  - Embryo Implantation Test and Live Birth Test
  - Histological and Immunohistochemical Staining
  - RNA Extraction, Reverse Transcription and Quantitative real-time PCR
  - Western blotting
- QUANTIFICATION AND STATISTICAL ANALYSIS

References

1. Capella-Allouc, S., Morsad, F., Rongières-Bertrand, C., Taylor, S., and Fernandez, H. (1999). Hysteroscopic treatment of severe Asherman's syndrome and subsequent fertility. Human Reproduction *14*, 1230-1233.
2. Vitale, S.G., Riemma, G., Carugno, J., Perez-Medina, T., Pacheco, L.A., Haimovich, S., Parry, J.P., Sardo, A.D.S., and De Franciscis, P. (2022). Postsurgical barrier strategies to avoid the recurrence of intrauterine adhesion formation after hysteroscopic adhesiolysis: a network meta-analysis of randomized controlled trials. American journal of obstetrics and gynecology *226*, 487-498. e488. https://doi.org/10.1016/j.ajog.2021.09.015.
3. Hooker, A.B., Lemmers, M., Thurkow, A.L., Heymans, M.W., Opmeer, B.C., Brölmann, H.A., Mol, B.W., and Huirne, J.A. (2014). Systematic review and meta-analysis of intrauterine adhesions after miscarriage: prevalence, risk factors and long-term reproductive outcome. Human reproduction update *20*, 262-278. https://doi.org/10.1093/humupd/dmt045.
4. Ma, J., Zhan, H., Li, W., Zhang, L., Yun, F., Wu, R., Lin, J., and Li, Y. (2021). Recent trends in therapeutic strategies for repairing endometrial tissue in intrauterine adhesion. Biomaterials Research *25*, 1-25. https://doi.org/10.1186/s40824-021-00242-6.
5. Zhu, R., Duan, H., Gan, L., and Wang, S. (2018). Comparison of intrauterine suitable balloon and Foley balloon in the prevention of adhesion after hysteroscopic adhesiolysis. BioMed Research International *2018*. https://doi.org/10.1155/2018/9494101.
6. Orhue, A., Aziken, M., and Igbefoh, J. (2003). A comparison of two adjunctive treatments

for intrauterine adhesions following lysis. International Journal of Gynecology & Obstetrics *82*, 49-56.

7. Yu, X., Yuhan, L., Dongmei, S., Enlan, X., and Tinchiu, L. (2016). The incidence of post-operative adhesion following transection of uterine septum: a cohort study comparing three different adjuvant therapies. European Journal of Obstetrics & Gynecology and Reproductive Biology *201*, 61-64. https://doi.org/10.1016/j.ejogrb.2016.01.039.
8. Kou, L., Jiang, X., Xiao, S., Zhao, Y.-Z., Yao, Q., and Chen, R. (2020). Therapeutic options and drug delivery strategies for the prevention of intrauterine adhesions. Journal of Controlled Release *318*, 25-37. https://doi.org/10.1016/j.jconrel.2019.12.007.
9. Abou-Ismail, M.Y., Sridhar, D.C., and Nayak, L. (2020). Estrogen and thrombosis: a bench to bedside review. Thrombosis research *192*, 40-51. https://doi.org/10.1016/j.thromres.2020.05.008.
10. Clemons, M., and Goss, P. (2001). Estrogen and the risk of breast cancer. New England Journal of Medicine *344*, 276-285.
11. Zhou, Z., Wang, H., Zhang, X., Song, M., Yao, S., Jiang, P., Liu, D., Wang, Z., Lv, H., and Li, R. (2022). Defective autophagy contributes to endometrial epithelial-mesenchymal transition in intrauterine adhesions. Autophagy *18*, 2427-2442. https://doi.org/10.1080/15548627.2022.2038994.
12. Leung, R.K.-K., Lin, Y., and Liu, Y. (2021). Recent advances in understandings towards pathogenesis and treatment for intrauterine adhesion and disruptive insights from single-cell analysis. Reproductive Sciences *28*, 1812-1826. https://doi.org/10.1007/s43032-020-00343-y.
13. Qi, J., Zhang, X., Zhang, S., Wu, S., Lu, Y., Li, S., Li, P., and Tan, J. (2023). P65 mediated UBR4 in exosomes derived from menstrual blood stromal cells to reduce endometrial fibrosis by regulating YAP Ubiquitination. Journal of nanobiotechnology *21*, 305. https://doi.org/10.1186/s12951-023-02070-3.
14. Lee, W.-L., Liu, C.-H., Cheng, M., Chang, W.-H., Liu, W.-M., and Wang, P.-H. (2021). Focus on the primary prevention of intrauterine adhesions: current concept and vision. International journal of molecular sciences *22*, 5175. https://doi.org/10.3390/ijms22105175.
15. Zhang, Y., Chen, X., Chen, S., Wei, C., Li, B., Wang, Z., Shen, X., and Lin, X. (2022). Intrauterine administration of G-CSF for promoting endometrial growth after hysteroscopic adhesiolysis: a randomized controlled trial. Human Reproduction *37*, 725-733. https://doi.org/10.1093/humrep/deac023.
16. Lu, C., Liu, M., Fu, H., Zhang, W., Peng, G., Zhang, Y., Cao, H., and Luo, L. (2015). Novel thermosensitive in situ gel based on poloxamer for uterus delivery. European Journal of Pharmaceutical Sciences *77*, 24-28. https://doi.org/10.1016/j.ejps.2015.05.014.
17. Naghshineh, E., Rouholamin, S., and Derakhshandeh, Z. (2023). Hormone therapy with or without platelet-rich plasma (PRP) for treatment Asherman syndrome; A randomized clinical trial. Advanced Biomedical Research *12*. https://doi.org/10.4103/abr.abr_411_21.
18. Shen, M., Duan, H., Lv, R., and Lv, C. (2022). Efficacy of autologous platelet-rich plasma in preventing adhesion reformation following hysteroscopic adhesiolysis: A randomized controlled trial. Reproductive BioMedicine Online *45*, 1189-1196.

https://doi.org/10.1016/j.rbmo.2022.07.003.
19. Peng, J., Li, M., Zeng, H., Zeng, Z., Huang, J., and Liang, X. (2020). Intrauterine infusion of platelet-rich plasma is a treatment method for patients with intrauterine adhesions after hysteroscopy. International Journal of Gynecology & Obstetrics *151*, 362-365. https://doi.org/10.1002/ijgo.13353.
20. Lin, Y., Qi, J., and Sun, Y. (2021). Platelet-rich plasma as a potential new strategy in the endometrium treatment in assisted reproductive technology. Frontiers in endocrinology *12*, 707584. https://doi.org/10.3389/fendo.2021.707584.
21. Zhou, J., Liu, Y., Liu, X., Wan, J., Zuo, S., Pan, T., Liu, Y., Sun, F., Gao, M., and Yu, X. (2023). Hyaluronic acid-based dual network hydrogel with sustained release of platelet-rich plasma as a diabetic wound dressing. Carbohydrate Polymers *314*, 120924. https://doi.org/10.1016/j.carbpol.2023.120924.
22. Cai, C., Zhu, H., Chen, Y., Yuan, X., Liu, H., and Yang, Z. (2023). Platelet-Rich Plasma Composite Organohydrogel with Water-Locking and Anti-Freezing to Accelerate Wound Healing. Advanced Healthcare Materials, 2301477. https://doi.org/10.1002/adhm.202301477.
23. Jiang, G., Li, S., Yu, K., He, B., Hong, J., Xu, T., Meng, J., Ye, C., Chen, Y., and Shi, Z. (2021). A 3D-printed PRP-GelMA hydrogel promotes osteochondral regeneration through M2 macrophage polarization in a rabbit model. Acta biomaterialia *128*, 150-162. https://doi.org/10.1016/j.actbio.2021.04.010.
24. Kim, M.K., Yoon, J.A., Yoon, S.Y., Park, M., Lee, W.S., Lyu, S.W., and Song, H. (2022). Human Platelet-Rich Plasma Facilitates Angiogenesis to Restore Impaired Uterine Environments with Asherman's Syndrome for Embryo Implantation and Following Pregnancy in Mice. Cells *11*. https://doi.org/10.3390/cells11091549.
25. Qian, Z., Wang, H., Bai, Y., Wang, Y., Tao, L., Wei, Y., Fan, Y., Guo, X., and Liu, H. (2020). Improving chronic diabetic wound healing through an injectable and self-healing hydrogel with platelet-rich plasma release. ACS Applied Materials & Interfaces *12*, 55659-55674. https://doi.org/10.1021/acsami.0c17142.
26. Smith, S.K. (2001). Regulation of angiogenesis in the endometrium. Trends in Endocrinology & Metabolism *12*, 147-151.
27. Lash, G.E., Innes, B.A., Drury, J.A., Robson, S.C., Quenby, S., and Bulmer, J.N. (2012). Localization of angiogenic growth factors and their receptors in the human endometrium throughout the menstrual cycle and in recurrent miscarriage. Human Reproduction *27*, 183-195.
28. Xiong, Y., Chen, L., Liu, P., Yu, T., Lin, C., Yan, C., Hu, Y., Zhou, W., Sun, Y., and Panayi, A.C. (2022). All-in-one: multifunctional hydrogel accelerates oxidative diabetic wound healing through timed-release of exosome and fibroblast growth factor. Small *18*, 2104229. https://doi.org/10.1002/smll.202303158.
29. Wu, J., Zhu, J., He, C., Xiao, Z., Ye, J., Li, Y., Chen, A., Zhang, H., Li, X., and Lin, L. (2016). Comparative study of heparin-poloxamer hydrogel modified bFGF and aFGF for in vivo wound healing efficiency. ACS applied materials & interfaces *8*, 18710-18721. https://doi.org/10.1021/acsami.6b06047.
30. Wang, S.Y., Kim, H., Kwak, G., Yoon, H.Y., Jo, S.D., Lee, J.E., Cho, D., Kwon, I.C., and Kim, S.H. (2018). Development of biocompatible HA hydrogels embedded with a new

synthetic peptide promoting cellular migration for advanced wound care management. Advanced science *5*, 1800852. https://doi.org/10.1002/advs.201800852.

31. Lv, H., Sun, H., Wang, L., Yao, S., Liu, D., Zhang, X., Pei, Z., Zhou, J., Wang, H., Dai, J., et al. (2023). Targeting CD301+ macrophages inhibits endometrial fibrosis and improves pregnancy outcome. EMBO molecular medicine *15*, e17601. https://doi.org/10.15252/emmm.202317601.
32. Zou, L., Huang, J., Zhang, Q., Mo, H., Xia, W., Zhu, C., and Rao, M. (2023). The humanin analogue (HNG) alleviates intrauterine adhesions by inhibiting endometrial epithelial cells ferroptosis: a rat model-based study. Human Reproduction *38*, 2422-2432. https://doi.org/10.1093/humrep/dead196.
33. Zhang, X., Zhang, S., Qi, J., Zhao, F., Lu, Y., Li, S., Wu, S., Li, P., and Tan, J. (2023). PDGFBB improved the biological function of menstrual blood-derived stromal cells and the anti-fibrotic properties of exosomes. Stem cell research & therapy *14*, 113. https://doi.org/10.1186/s13287-023-03339-y.
34. Li, J., Qi, J., Yao, G., Zhu, Q., Li, X., Xu, R., Zhu, Z., Zhao, H., Wang, Y., and Ding, Y. (2021). Deficiency of sirtuin 1 impedes endometrial decidualization in recurrent implantation failure patients. Frontiers in Cell and Developmental Biology *9*, 598364. https://doi.org/10.3389/fcell.2021.598364.
35. Zhao, H., Hu, S., Qi, J., Wang, Y., Ding, Y., Zhu, Q., He, Y., Lu, Y., Yao, Y., and Wang, S. (2022). Increased expression of HOXA11-AS attenuates endometrial decidualization in recurrent implantation failure patients. Molecular Therapy *30*, 1706-1720. https://doi.org/10.1016/j.ymthe.2022.01.036.
36. Salma, U., Xue, M., Ali Sheikh, M.S., Guan, X., Xu, B., Zhang, A., Huang, L., and Xu, D. (2016). Role of transforming growth factor-β1 and smads signaling pathway in intrauterine adhesion. Mediators of inflammation *2016*. https://doi.org/10.1155/2016/4158287.
37. Zhou, Q., Wu, X., Hu, J., and Yuan, R. (2018). Abnormal expression of fibrosis markers, estrogen receptor α and stromal derived factor-1/chemokine (C-X-C motif) receptor-4 axis in intrauterine adhesions. International journal of molecular medicine *42*, 81-90. https://doi.org/10.3892/ijmm.2018.3586.
38. Li, B., Zhang, Q., Sun, J., and Lai, D. (2019). Human amniotic epithelial cells improve fertility in an intrauterine adhesion mouse model. Stem cell research & therapy *10*, 257. https://doi.org/10.1186/s13287-019-1368-9.
39. Neeman, M., Gilad, A.A., Dafni, H., and Cohen, B. (2007). Molecular imaging of angiogenesis. Journal of Magnetic Resonance Imaging: An Official Journal of the International Society for Magnetic Resonance in Medicine *25*, 1-12.
40. Lin, J., Wang, Z., Huang, J., Tang, S., Saiding, Q., Zhu, Q., and Cui, W. (2021). Microenvironment-protected exosome-hydrogel for facilitating endometrial regeneration, fertility restoration, and live birth of offspring. Small *17*, 2007235. https://doi.org/10.1002/smll.202007235.
41. Gurtner, G.C., Werner, S., Barrandon, Y., and Longaker, M.T. (2008). Wound repair and regeneration. Nature *453*, 314-321.
42. Zhang, D., Du, Q., Li, C., Ding, C., Chen, J., He, Y., Duan, T., Feng, Q., Yu, Y., and Zhou, Q. (2023). Functionalized human umbilical cord mesenchymal stem cells and injectable

HA/Gel hydrogel synergy in endometrial repair and fertility recovery. Acta Biomaterialia *167*, 205-218. https://doi.org/10.1016/j.actbio.2023.06.013.

43. Miki, D., Dastgheib, K., Kim, T., Pfister-Serres, A., Smeds, K.A., Inoue, M., Hatchell, D.L., and Grinstaff, M.W. (2002). A photopolymerized sealant for corneal lacerations. Cornea *21*, 393-399.
44. Shi, W., Hass, B., Kuss, M.A., Zhang, H., Ryu, S., Zhang, D., Li, T., Li, Y.-l., and Duan, B. (2020). Fabrication of versatile dynamic hyaluronic acid-based hydrogels. Carbohydrate polymers *233*, 115803. https://doi.org/Fabrication of versatile dynamic hyaluronic acid-based hydrogels.
45. Lv, H., Nan, Z., Jiang, P., Wang, Z., Song, M., Ding, H., Liu, D., Zhao, G., Zheng, Y., and Hu, Y. (2019). Vascular endothelial growth factor 165 inhibits pro-fibrotic differentiation of stromal cells via the DLL4/Notch4/smad7 pathway. Cell Death & Disease *10*, 681. https://doi.org/10.1038/s41419-019-1928-z.

STAR Methods

KEY RESOURCES TABLE

REAGENT or RESOURCE	**SOURCE**	**IDENTIFIER**
Chemicals		
HA	Aladdin Scientific	H131007
MA	TargetMol	T65288
PBA	Aladdin Scientific	P107045
PVA	Aladdin Scientific	P139548
ELISA kits		
VEGF	R&D	DVE00
EGF	R&D	DEG00
PDGF	R&D	DHD00C
Antibodies for IHC		
COL1A1	Servicebio Technology	Cat#: GB11022-3-100
α-SMA	Cell Signaling Technology	Cat#: 19245; RRID: AB_2734735
vWF	Servicebio Technology	Cat#: GB11020
CD31	R&D	Cat#: AF3628; RRID: AB_2161028
Antibodies for Western blotting		
GAPDH	Proteintech Group Inc	Cat#: 60004-1-Ig; RRID: AB_2107436
CTGF	Santa Cruz Biotechnology	Cat#: sc-365970; RRID: AB_10917259
COL1A1	Cell Signaling Technology	Cat#: 72026; RRID: AB_2904565
α-SMA	Cell Signaling Technology	Cat#: 19245; RRID: AB_2734735
SMAD2/3	Cell Signaling Technology	Cat#: 8685; RRID: AB_10889933
p-SMAD2/3 (Ser465/Ser467)	Cell Signaling Technology	Cat#: 8828; RRID:
Primer sequences		
GAPDH (Homo sapiens)	Sangon Biotech	F: GTCTCCTCTGACTTCAACAGCG B: ACCACCCTGTTGCTGTAGCCAA
COL1A1 (Homo sapiens)	Sangon Biotech	F: GATTCCCTGGACCTAAAGGTGC B: AGCCTCTCCATCTTTGCCAGCA
α-SMA (Homo sapiens)	Sangon Biotech	F: CTATGAGGGCTATGCCTTGCC B: GCTCAGCAGTAGTAACGAAGGA
CTGF (Homo sapiens)	Sangon Biotech	F: CAGCATGGACGTTCGTCTG B: AACCACGGTTTGGTCCTTGG
VEGFA (Homo sapiens)	Sangon Biotech	F: TTGCCTTGCTGCTCTACCTCCA B: GATGGCAGTAGCTGCGCTGATA
PDGFA (Homo sapiens)	Sangon Biotech	F: CAGCGACTCCTGGAGATAGACT B: CGATGCTTCTCTTCCTCCGAATG
FSTL1 (Homo sapiens)	Sangon Biotech	F: TCGCATCATCCAGTGGCTGGAA B: TCACTGGAGTCCAGGCGAGAAT
ANGPT2 (Homo sapiens)	Sangon Biotech	F: ATTCAGCGACGTGAGGATGGCA B: GCACATAGCGTTGCTGATTAGTC

RESOURCE AVAILABILITY

Lead contact

Lead contact Further information and requests for resources should be directed to and will be fulfilled by the lead contact, Yun Sun (syun163@163.com)

Materials availability

Hydrogel reagents and peptides described in the manuscript are commercially available.

Data and code availability

- All data is presented within this paper. This paper does not report original code.
- Any additional information required to reanalyze the data reported in this paper is available from the lead contact upon request.

EXPERIMENTAL MODEL AND SUBJECT DETAILS

Endometrial tissue acquisition, cell isolation and cell culture

All participants were enrolled with written informed consent approved by the Ethics Committee of Ren Ji Hospital, affiliated with Shanghai Jiao Tong University School of Medicine (Approval No. KY2021-211-B). The endometrial biopsies were collected from pipelle biopsies from reproductive age women (n=16, age 20-40).

Primary human endometrial stromal cells (HESCs) were enzymatically isolated from endometrial biopsy samples using a selective attachment method. The samples underwent an initial PBS rinse followed by digestion with 0.1% collagenase type I at 150 rpm for 40 minutes, and with 0.1% deoxyribonuclease I (Sigma-Aldrich) for 15 minutes. The mixture was filtered in a sequential manner through 180 μm and 40 μm cell sieves, permitting only HESCs to pass through. HESCs were cultured in Phenol Redfree Dulbecco's modified Eagle's medium (DMEM)/F-12 (Gibco) supplemented with 10% charcoal-stripped fetal bovine serum (Biological Industries) and 1% penicillin-streptomycin-neomycin antibiotic mixture (Thermo Fisher Scientific) at 37℃ in a 5% CO_2 atmosphere. Cell purity was tested routinely by immunofluorescence staining for cytokeratin and vimentin.

Human umbilical vein endothelial cells (HUVECs) were procured from the American Type Culture Collection and cultured in RPMI-1640 with 1% penicillin-streptomycin-neomycin, and 10% fetal bovine serum at 37 °C in a 5% CO_2 incubator. The conditioned medium was prepared by immersing various hydrogels in DMEM with 1% penicillin-streptomycin-neomycin for two days before using.

In Vivo IUA Model Construction and Treatment

This study utilized Sprague-Dawley (SD) rats procured from Beijing Vital River Laboratory Animal Technology. All animal experiments adhered to the Guide for the Care and Use of Laboratory Animals (NIH Publications No. 80-23) and received approval from the Animal Care Committee of Ren Ji Hospital, Shanghai Jiao Tong University School of Medicine (RJ2022-0829).

The animals were housed in a facility with controlled temperature (20–26 °C) and humidity (40–70%), following a 12-hour light/dark cycle (lights on at 6 am), and were provided with standard laboratory sterile feed and pure water. Vaginal smears were collected daily between 8-10 a.m.

The IUA rat model was established by injecting 95% ethanol into the uterus, as previously described[40]. Female Sprague-Dawley rats (200–220 g, 8 weeks old) with normal estrous cycles were randomly divided into five groups: Control (CTRL), Ethanol (ETOH), Gel (GEL), Platelet-Rich Plasma (PRP), and PRP in Gel (PRP@GEL). Rats were anesthetized via intraperitoneal injection of a mixture of tiletamide (12.5mg/kg), zolazepam (12.5mg/kg), and xylazine(5mg/kg). The CTRL group consisted of sham-operated rats, where 100 μL of PBS was injected into the uterine horns. The ETOH, GEL, PRP, and PRP@GEL groups were subjected to endometrial injury by injecting 100 μL of 95% ethanol into the uterine horns. The distal portions of the uterus were clamped with vascular clamps to its full capacity and retained for 60 seconds. The clamps were then released, and the uterine cavity was gently flushed with PBS to remove residual ethanol. For the GEL, PRP, and PRP@GEL groups, 100 μL of HAMA-PBA-PVA gel, 100 μL of diluted PRP (containing 42.8 μL PRP), and PRP@GEL (containing 42.8 μL PRP) were respectively injected into the uterine cavity post-PBS flush. The muscle layer and skin were then sutured using 4–0 non-absorbable sutures. Fourteen rats were euthanized 14 days post-surgery, and uterine tissues were harvested for further mechanistic exploration. Sixteen additional rats were used for subsequent embryo implantation and live birth tests.

METHOD DETAILS

Materials and synthesis

Fabrication of HAMA-PBA

HAMA was produced following the procedure in a previous report [43]. To summarize, 2 g of HA was dissolved by stirring in 10.0 mL of deionized water (DI). Next, 7 mL of methacrylic anhydride were added drop by drop while maintaining the pH level of the mixture between 8-10. The reaction was allowed to occur in darkness for 24 hours. Subsequently, the reaction mixture was washed with ethanol, dialyzed with DI water for five days, and freeze-dried.

HAMA-PBA was produced based on a previously reported procedure [44]. Initially, 1 g of HAMA was dissolved in 200 mL of DI water by stirring. Subsequently, 0.5 g of 3-aminomethyl PBA and 1.5 g of 4(4,6-dimethoxy-1,3,5-triazin-2-yl)-4-methyl-morpholinium chloride were added to the HAMA solution. The mixture's pH was kept at 6.5 and stirred for 72 hours at room temperature. Subsequently, the mixture underwent dialysis with DI water for five days and freeze-drying.

Proton nuclear magnetic resonance analysis of HAMA-PBA conjugates

^{1}H NMR analysis was carried out on a 500 MHz Bruker NMR system and analyzed with MestReNova. The polymer conjugates were dissolved in D_2O at a concentration of 5 mg/mL for NMR data acquisition. The chemical shifts were calibrated with respect to the D2O solvent peak

(4.78 ppm at 25 °C).

Fabrication of HAMA-PBA-PVA hydrogels

HAMA-PBA was dissolved in PBS (pH 8.5) to obtain a 6% (w/v) solution (precursor solution A), while PVA was dissolved in PBS (pH 8.5) to obtain a 1% (w/v) solution (precursor solution B). HAMA-PBA-PVA hydrogels were prepared by mixing the precursor solutions using a double-barreled syringe at a volume ratio of 1:1, at room temperature and a pH of 8.5. The mixed solution from the double-barrelled syringe was exposed to a 365 nm, 400 W long-wavelength ultraviolet (UV) lamp (Intelliray 400, Uvitron) for 20 seconds.

Fabrication of the PRP@HAMA-PBA-PVA hydrogels

HAMA-PBA, Lithium phenyl-2,4,6-trimethylbenzoylphosphinate (LAP) and Calcium Chloride ($CaCl_2$) was dissolved in PBS (pH 8.5) to obtain a 6% (w/v) HAMA-PBA, 0.2% LAP and 1% $CaCl_2$ mixture solution as precursor solution A. The precursor solution B was prepared by dissolving PVA in PRP to get a 1%(w/v) PVA-PRP mixture solution as precursor solution B. PRP@HAMA-PBA-PVA hydrogels were produced by combining precursor solution A and precursor solution B through a double-barrelled syringe in a 1:1 volume ratio at pH 8.5, under room temperature conditions.. Further, the mixed solution from customized double-barreled syringe was exposed to UV light for 20 s. The hydrogels without UV irradiation were denoted as single-network PRP@HAMA-PBA-PVA and the hydrogels after UV irradiation were denoted as double-network PRP@HAMA-PBA-PVA. In the following *in vitro* and *in vivo* experiments, HAMA-PBA-PVA hydrogel and PRP@HAMA-PBA-PVA hydrogel were denoted as GEL and PRP@GEL.

Characteristics of the hydrogels

Rheological properties of the hydrogels

The rheological experiments were performed utilizing a TA Instruments AR-G2 stress-controlled rheometer equipped with a 40 mm (diameter) 2° cone geometry, gap size being 53 μm. An oscillatory strain (γ) amplitude sweep was conducted with a fixed angular frequency (ω) of 10 rad/s and γ values ranging from 1 to 1000%. Subsequently, a dynamic time sweep was performed at a constant frequency of 10 rad/s and a strain of 1%. Subsequently, the consistency of the self-repairing mechanism was evaluated via a cyclic strain study, where γ was varied between 1% and 1000% for three cycles at a constant frequency of 10 rad/s.

Injectability studies and degradation of the hydrogels

The hydrogel's injectability was tested on a macroscale. First, precursor solution A, precursor solution B of PRP@GEL and crystal violetto were mixed all together and loaded into a 1 mL syringe. After being exposed to UV light, the syringe was sealed with a 21-gauge needle to assess whether the hydrogel could be expelled through the needle into a plastic dish by manually

pressing the syringe plunger.

The degradation of the hydrogel was also tested on a macroscale. First, precursor solution A, precursor solution B of PRP@GEL and crystal violetto were mixed all together and loaded into a 1 mL syringe. After irradiated with UV lamp, the hydrogels were incubated in PBS solution at PH 7.4 at 37 °C. And the samples were being agitated in a shaker at 37 °C, 80 rpm.

Scanning electron microscopy (SEM)

The structure of the hydrogel was observed by SEM. The hydrogel before UV irradiation and after UV irradiation were both characterized. The hydrogel samples were lyophilised beforehand and then positioned on the objective tables prior to gold sputtering. The specimens were analysed, and pictures were captured using Thermo Quattro S.

Preparation of PRP

Blood samples were procured from healthy 8-week-old SD rats. A two-step centrifugation process was utilized to extract PRP. Specifically, 8 mL of whole blood was drawn from each rat under general anesthesia. The samples were then centrifuged at 1000g for 10 minutes, resulting in a separation into three layers: plasma, leukocytes/platelet, and erythrocytes, from top to bottom respectively. The upper leukocyte/platelet layer and plasma layer were transferred to a new centrifuge tube for a second centrifugation at 2000g for 10 minutes. The remaining supernatant plasma was discarded, leaving behind 0.5 mL of plasma with precipitated platelets, which was thoroughly mixed and identified as PRP. Erythrocytes were meticulously removed to minimize interference. Platelet counts in PRP were ascertained using an automated counter.

***In Vitro* Growth Factor Release Kinetics**

The release behavior of growth factors from the PRP@Gel hydrogels were analyzed as following.

Specifically, 1 mL of the PRP@Gel hydrogel sample was immersed in 1 mL of PBS in a 24-well plate and then stirred at 80 rpm and maintained at 37 ℃. Every 24 hours, 300 ml of mixture liquid was aspirated and replaced with an equal volume of PBS. The collected liquid specimens were preserved at -80℃ for subsequent analysis. We used the quantitative Enzyme-linked Immunosorbent Assay (ELISA) Kits (R&D Systems) to measure the levels of human PDGF, VEGF, and EGF following the reagent protocols.

***In Vitro* Cell Proliferation Experiments**

Cell proliferation was assessed using a CCK-8 assay kit (Dojindo) and an EdU Cell Proliferation Kit with Alexa Fluor 594 (Beyotime), following the manufacturers' guidelines. For the CCK-8 assay, the optical density of each well at 450 nm was measured with a microplate reader (Thermo Fisher) after 24, 48, and 72 hours of culture in the conditioned medium. For the EdU assay, cells were seeded in 96-well plates and cultured in the conditioned medium at 37°C in a humidified 5%

CO_2 incubator for 24 hours. EdU (final concentration 10uM) was added at the 12th hour of co-culture, and incubation continued for an additional 12 hours. The cells were fixed, permeabilised, blocked and stained in accordance with the instructions provided. Images were captured using a fluorescence microscope (LSM800) and analyzed with Image J software.

***In Vitro* Fibrosis and Anti-fibrosis Experiments**

HESCs were seeded in a 6-well plate and incubated at 37°C for 48 hours in 10% FBS-DMEM/F12 medium containing 10ng/mL recombinant human TGF-β1 (PeproTech)[45]. Following TGF-β1 treatment, the culture medium was replaced with conditioned medium, and the cells were incubated for an additional 24 hours. Subsequently, RNA and protein were extracted from the HESCs for fibrosis analysis.

***In Vitro* Angiogenesis Experiments**

Wound Scratch Assay

HUVECs were seeded in 24-well plates and cultured for 24 hours. A scratch wound was produced on the cell surface using a pipette tip, after which the HUVECs were incubated in the conditioned medium. The scratch area was photographed at 0 and 12 hours post-incubation. The scratch healing rate was calculated by comparing the closed area with the initial wound area.

Transwell Assay of Cell Invasion

HUVECs were seeded onto the inner surface of the upper Transwell insert that was precoated with Matrigel, with the conditioned medium added to the lower chamber. Following a 24-hour incubation, the wells were treated with 4% paraformaldehyde and stained with crystal violet dye (Beyotime) and images were captured using microscopy and quantified using ImageJ software.

Tube Formation Assays

Each well of a 96-well plate was coated with 50 μL of Matrigel (ABW, Shanghai, China) and incubated at 37℃ for 30 minutes. Subsequently, HUVECs were seeded onto the Matrigel-coated surface using 100 μL of conditioned medium. After a 6-hour incubation, the HUVECs were stained with Calcein-AM (MCE, Shanghai, China) for 30 minutes, and images were captured using fluorescence microscopy. Various tube formation indicators were quantified using ImageJ software.

Embryo Implantation Test and Live Birth Test

Fourteen days post-operation, male Sprague-Dawley mice were paired with the female rats in a 1:1 ratio, and successful mating was confirmed via vaginal smear. The rats were euthanized 14 days post-coitum (dpc), and the uteri were collected for analysis of embryo implantation numbers and rates. The number and rate of live births were observed approximately 21-23 days into gestation, and the offspring's weight was measured.

Histological and Immunohistochemical Staining

Human endometrial and rat uterine tissues were fixed with 4% paraformaldehyde and embedded in wax following gradient dehydration. The tissues were then sectioned into 10 μm-thick slices for subsequent experiments. These tissue sections underwent Hematoxylin and Eosin (H&E) and Masson's trichrome staining according to the provided instructions. The distance from the inner layer of the rat endometrium to the myometrium was measured in the H&E stained images of three uterine cross-sections, and an average value was calculated. Collagen deposition was analyzed using Image J software based on the images from Masson's trichrome staining. Endometrial fibrosis and angiogenesis levels were assessed through immunohistochemical staining. The sections were deparaffinized, rehydrated, and incubated with various primary antibodies overnight at 4 °C. On second day, the sections were incubated with secondary antibodies at room temperature for one hour. Subsequently, a DAB chromogenic reaction and hematoxylin staining were performed. The images were then captured using an optical microscope and analyzed using Image J software.

RNA Extraction, Reverse Transcription and Quantitative real-time PCR

Tissues and cells were processed with TRIzol reagent (Invitrogen) to extract total RNA. The concentration and quality of the extracted RNA were assessed using a NanoDrop ND-2000 spectrophotometer (Thermo-Fisher Scientific). Subsequently, reverse transcription was carried out using the PrimeScript RT reagent kit (TaKaRa), utilizing 500 ng of the total RNA. Quantitative real-time polymerase chain reaction was conducted using 2×SYBR Green qPCR Master Mix (Low ROX) (Bimake) using ABI Prism System (Applied Biosystems). All qRT-PCR reactions were conducted in triplicate, and the final reaction volume was 10 μL. The relative mRNA levels were calculated using the $2^{(-\Delta\Delta Ct)}$ method, with GAPDH as an internal control.

Western blotting

Protein was extracted from cells using RIPA lysis buffer (Cwbio), supplemented with a phosphatase inhibitor (Active Motif) and a protease inhibitor cocktail (Roche). The protein (40 mg) from each sample was electrophoresed on a precast 4-12% Bis-Tris gradient gel (Tanon) and then transferred onto a nitrocellulose blot. The membrane was blocked with 5% nonfat milk for one hour. Subsequently, primary antibodies were added and the membrane was incubated overnight at 4 C. The next day, the membrane was washed and incubated with the corresponding horseradish peroxidase-conjugated secondary antibody (Proteintech) for one hour. The peroxidase activity bands were determined by using an enhanced chemiluminescent detection kit (Epizyme) and recorded with a G-Box chemiluminescence image capture system (Syngene). The identical blot was additionally examined using GAPDH (1:5000) as an internal control.

QUANTIFICATION AND STATISTICAL ANALYSIS

Utilizing GraphPad Prism 9.0 and SPSS 22.0, statistical analysis was performed. When comparing two groups, the student's t-test was utilized, and when comparing three or more groups, a one-way ANOVA with Bonferroni tests was used, with a significance level of $p < 0.05$ (*P < 0.05, **P < 0.01, ***P < 0.001). Standard error of the mean (SEM) ± mean is how the data are displayed.

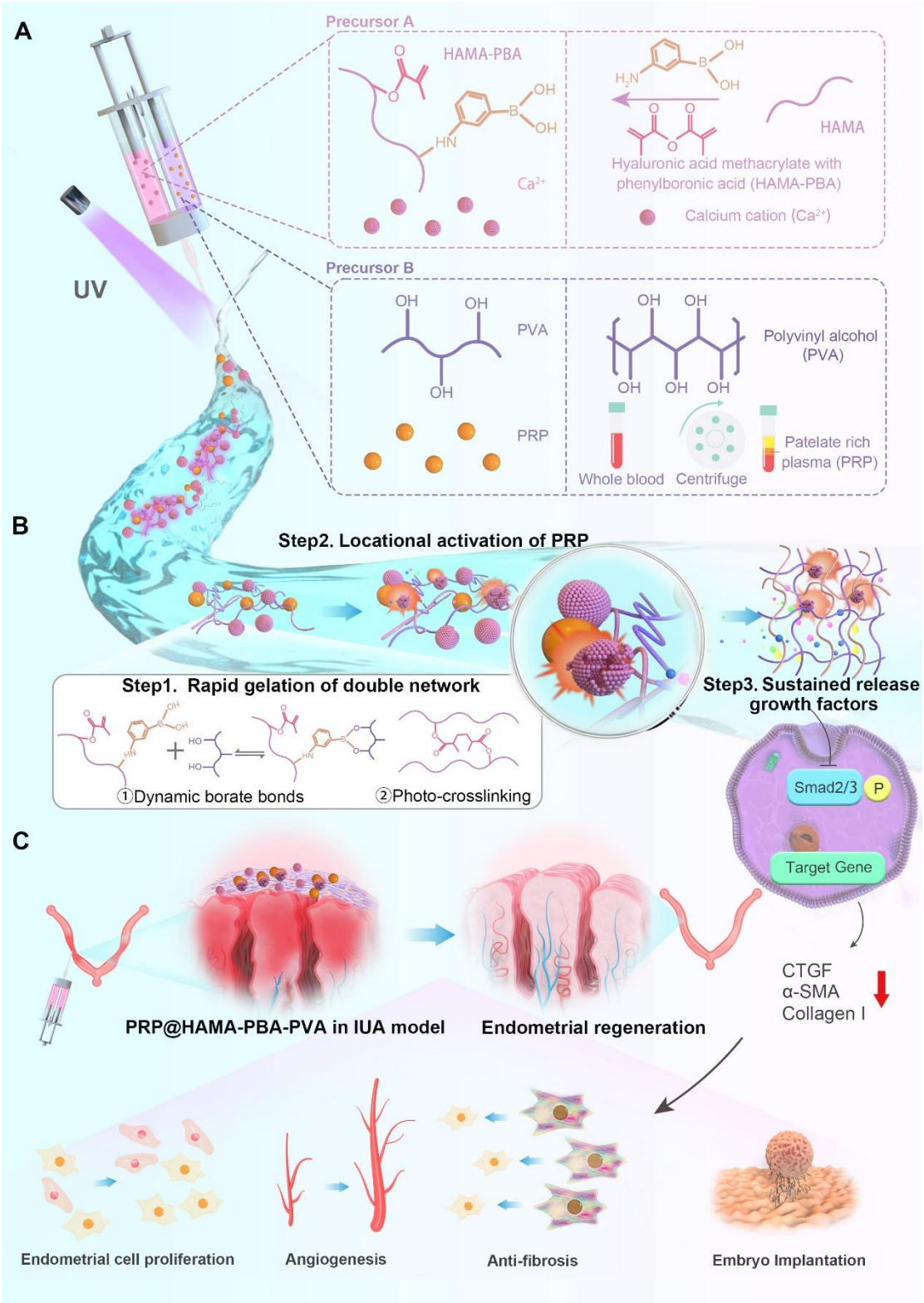

Figure 1

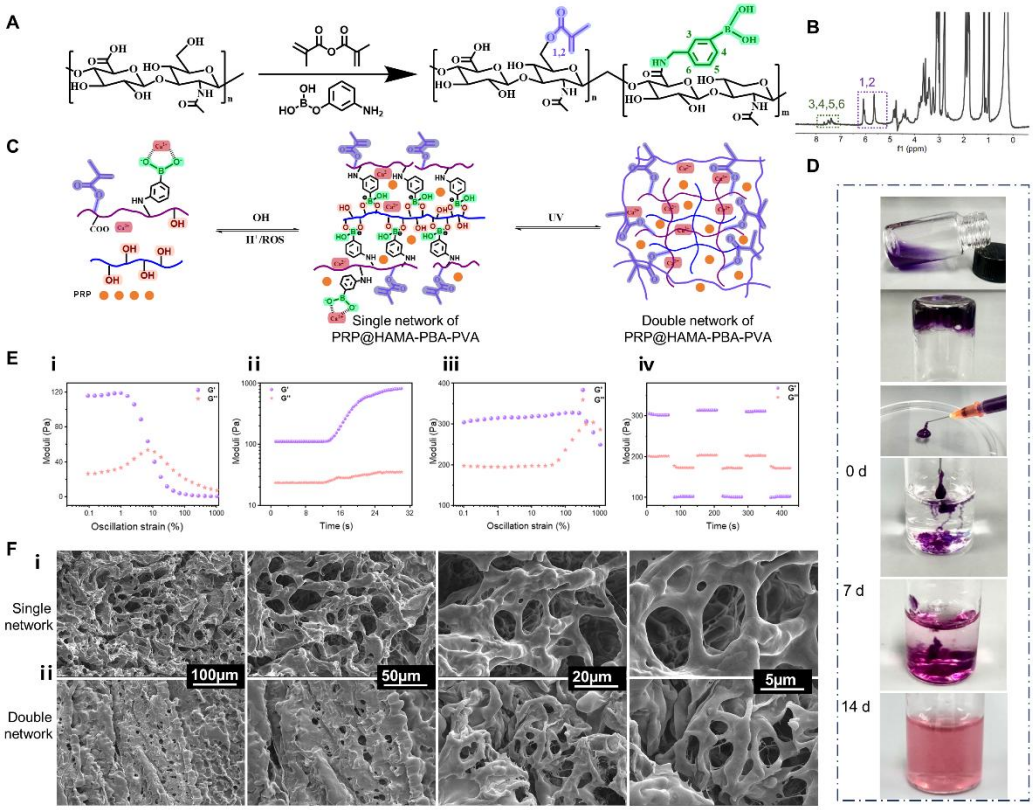
A
B
1,2
3,4,5,6
f1 (ppm)
C
PRP
OH
H+/ROS
UV
Single network of
PRP@HAMA-PBA-PVA
Double network of
PRP@HAMA-PBA-PVA
D
0 d
7 d
14 d
E
i
ii
iii
iv
Moduli (Pa)
Oscillation strain (%)
Time (s)
F
Single network
Double network
100μm
50μm
20μm
5μm

Figure 2

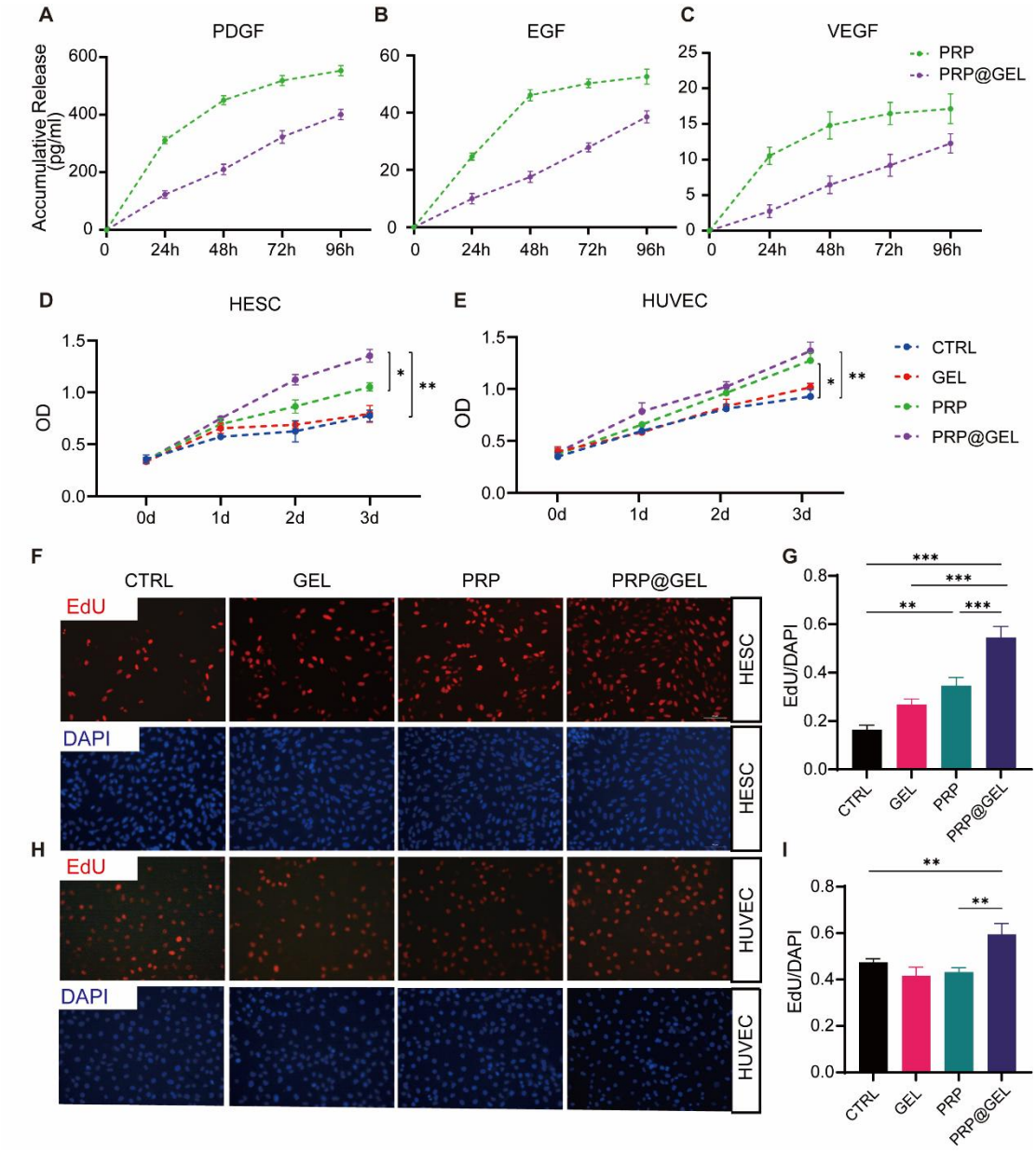
A
PDGF
B
EGF
C
VEGF
Accumulative Release (pg/ml)
PRP
PRP@GEL
0
24h
48h
72h
96h
D
HESC
E
HUVEC
OD
0d
1d
2d
3d
CTRL
GEL
PRP
PRP@GEL
F
EdU
DAPI
HESC
HUVEC
G
EdU/DAPI
H
I

Figure 3

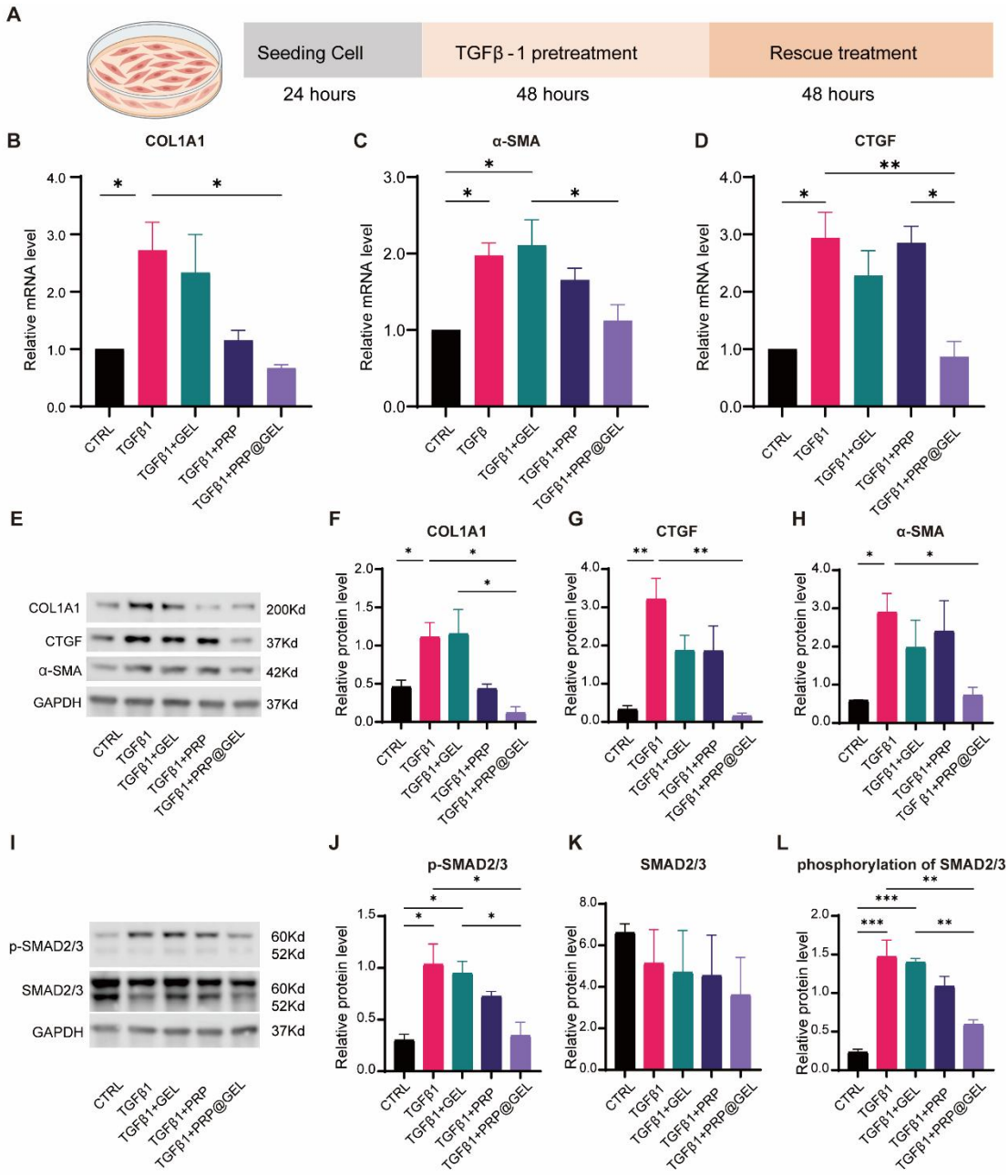
A
Seeding Cell
TGFβ-1 pretreatment
Rescue treatment
24 hours
48 hours
48 hours
B
COL1A1
C
α-SMA
D
CTGF
Relative mRNA level
CTRL
TGFβ1
TGFβ
TGFβ1+GEL
TGFβ1+PRP
TGFβ1+PRP@GEL
E
COL1A1
CTGF
α-SMA
GAPDH
200Kd
37Kd
42Kd
37Kd
F
COL1A1
G
CTGF
H
α-SMA
Relative protein level
I
p-SMAD2/3
SMAD2/3
GAPDH
60Kd
52Kd
60Kd
52Kd
37Kd
J
p-SMAD2/3
K
SMAD2/3
L
phosphorylation of SMAD2/3

Figure 4

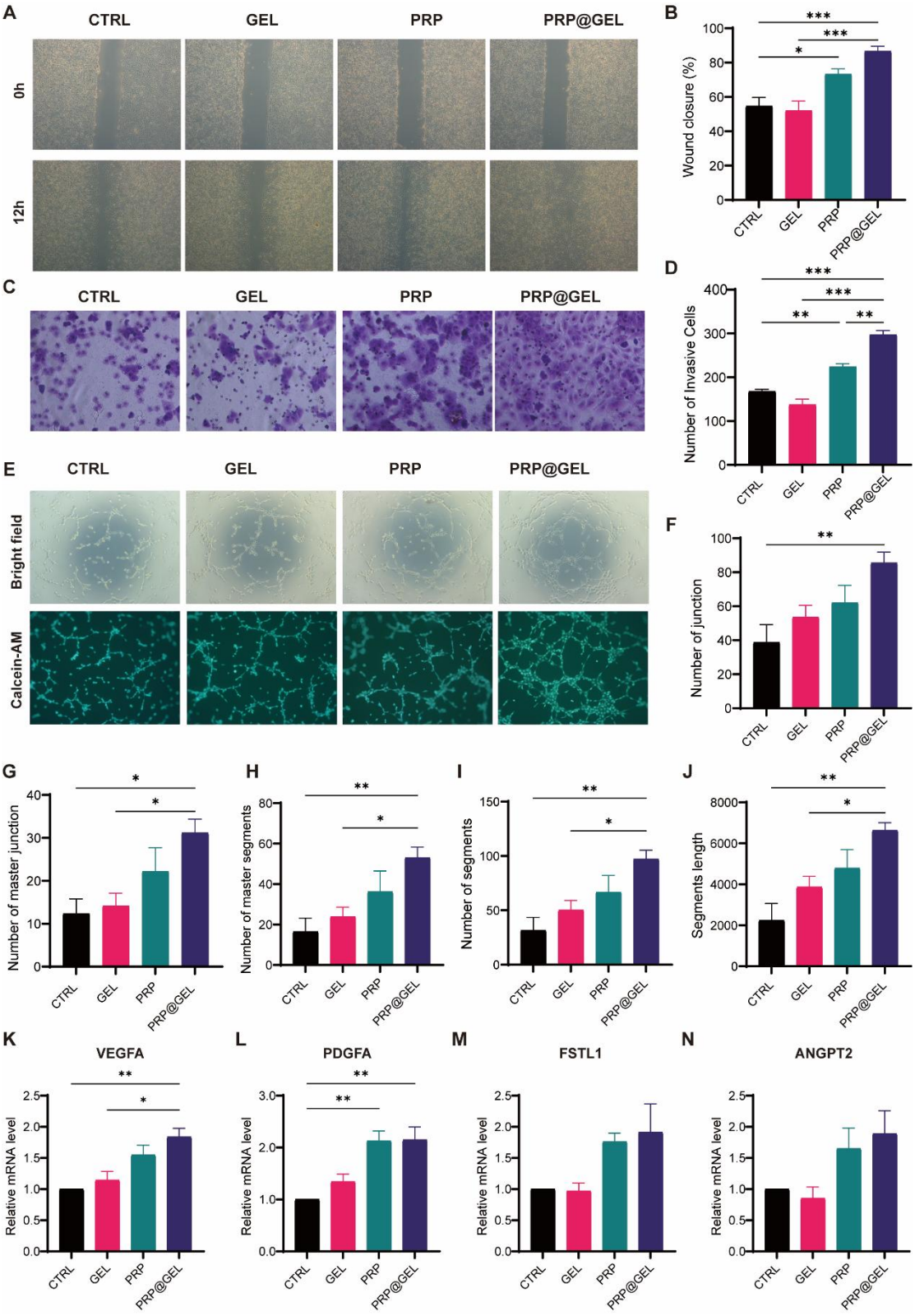
A
CTRL
GEL
PRP
PRP@GEL
0h
12h
B
Wound closure (%)
C
D
Number of Invasive Cells
E
Bright field
Calcein-AM
F
Number of junction
G
Number of master junction
H
Number of master segments
I
Number of segments
J
Segments length
K
VEGFA
L
PDGFA
M
FSTL1
N
ANGPT2
Relative mRNA level

Figure 5

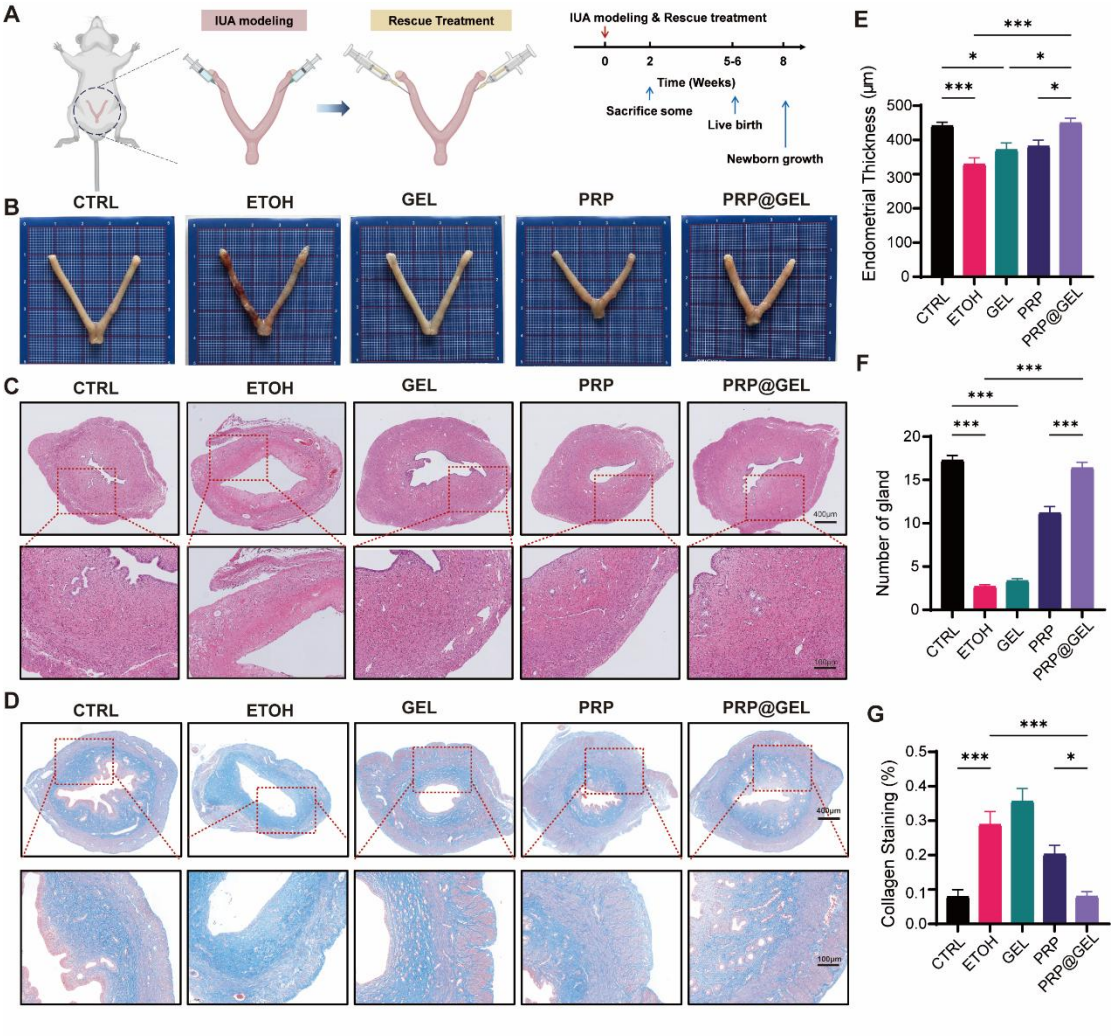
A
IUA modeling
Rescue Treatment
IUA modeling & Rescue treatment
0
2
5-6
8
Time (Weeks)
Sacrifice some
Live birth
Newborn growth
B
CTRL
ETOH
GEL
PRP
PRP@GEL
C
CTRL
ETOH
GEL
PRP
PRP@GEL
400μm
100μm
D
CTRL
ETOH
GEL
PRP
PRP@GEL
400μm
100μm
E
Endometrial Thickness (μm)
0
100
200
300
400
500
***
*
*
***
*
CTRL
ETOH
GEL
PRP
PRP@GEL
F
Number of gland
0
5
10
15
20
***
***
***
***
CTRL
ETOH
GEL
PRP
PRP@GEL
G
Collagen Staining (%)
0.0
0.1
0.2
0.3
0.4
0.5
***
***
*
CTRL
ETOH
GEL
PRP
PRP@GEL

Figure 6

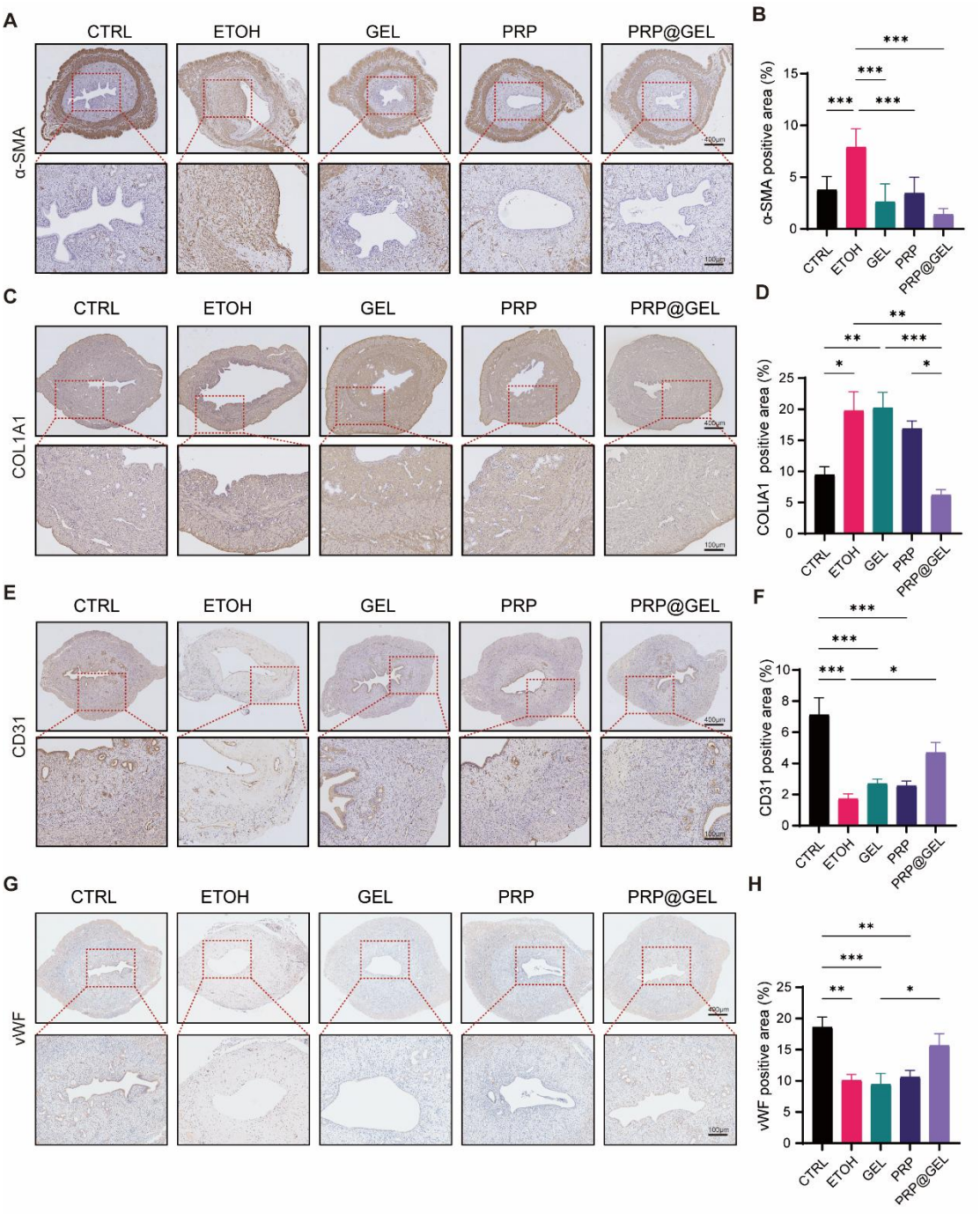
A
CTRL
ETOH
GEL
PRP
PRP@GEL
α-SMA
B
α-SMA positive area (%)
C
COL1A1
D
COLIA1 positive area (%)
E
CD31
F
CD31 positive area (%)
G
vWF
H
vWF positive area (%)

Figure 7

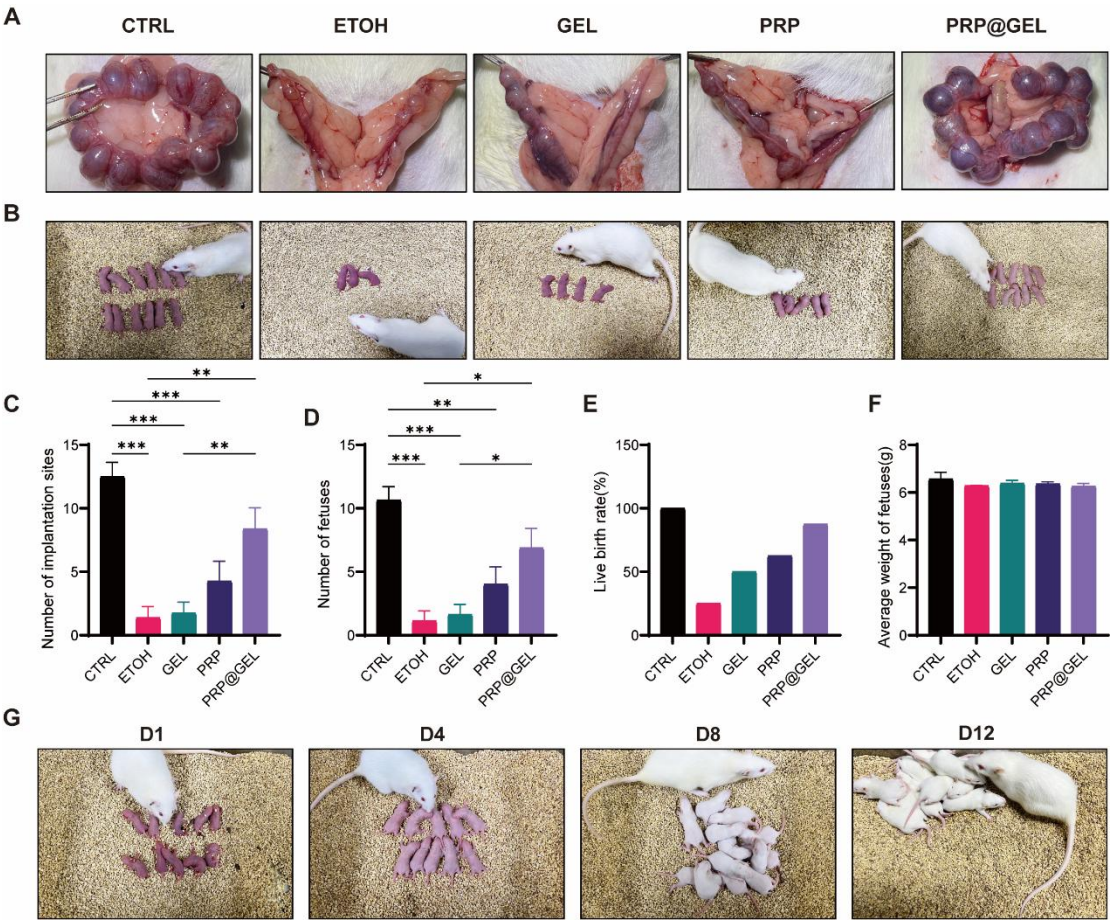
A
CTRL
ETOH
GEL
PRP
PRP@GEL
B
C
Number of implantation sites
D
Number of fetuses
E
Live birth rate(%)
F
Average weight of fetuses(g)
G
D1
D4
D8
D12

Figure 8